3D Isotope Density Measurements by Energy-Resolved Neutron Imaging

Adrian Simon Losko
Los Alamos National Laboratory
Sven Vogel (sven@lanl.gov)
Los Alamos National Laboratory

Research Article

Keywords: atoms, electron, X-rays, finger-print, microprobe map

Posted Date: October 27th, 2021

DOI: https://doi.org/10.21203/rs.3.rs-997052/v1

Version of Record: A version of this preprint was published at Scientific Reports on April 22nd, 2022. See the published version at https://doi.org/10.1038/s41598-022-10085-3.

Abstract

Tools for three-dimensional elemental characterization are available on length scales ranging from individual atoms, using electrons as a probe, to micrometers with X-rays. However, for larger volumes up to millimeters or centimeters, quantitative measurements of elemental or isotope densities were hitherto only possible on the surface. Here, a novel quantitative elemental characterization method based on energy-resolved neutron imaging, utilizing the known neutron absorption cross sections with their 'finger-print' absorption resonance signatures, is demonstrated. Enabled by a pixilated time-of-flight neutron transmission detector installed at an intense short-pulsed spallation neutron source, for this demonstration 3.25 million state-of-the-art nuclear physics neutron transmission analyses were conducted to derive isotopic densities for five isotopes in 3D in a volume of 0.25 cm^3. The tomographic reconstruction of the isotope densities provides elemental maps similar to X-ray microprobe maps for any cross-section in the probed volume. The bulk isotopic density of a U-20Pu-10Zr-3Np-2Am nuclear transmutation fuel sample was measured, agrees well with mass-spectrometry and is evidence of the accuracy of the method.

1. Introduction

Characterizing the elemental composition of materials is of great interest in scientific disciplines ranging from mineralogy to energy materials. Well established methods like X-ray fluorescence [1] provide *elemental* compositions on the surface and methods such as laser ablation inductively coupled plasma mass spectrometry [2] allow *isotopic* concentration measurements on the surface. Knowledge of the *three-dimensional* elemental concentration is desirable in many cases and electron- and X-ray based methods were developed for nanometer [3] and micrometer [4, 5] length scales. Destructive methods, analyzing nanometer scale volumes by removing atom by atom, also exist [6]. All of these techniques require significant sample preparation. While millimeter to centimeter scale 3D visualizations of cracks and average attenuation, without elemental sensitivity, is provided by hard X-ray [7, 8] or thermal neutron tomography [9], a method for three-dimensional element or isotope density measurements on millimeter or centimeter length-scales was hitherto missing. Here, a novel quantitative method is presented based on energy-resolved neutron imaging, utilizing the known neutron absorption cross-sections with their 'finger-print' absorption resonance signatures. The method is enabled by a pixilated (512 × 512 pixels) time-of-flight neutron transmission detector [10] installed at an intense short-pulsed spallation neutron source [11]. For the demonstration reported here, 3.25 million state-of-the-art nuclear physics neutron transmission analyses were conducted to derive isotopic densities for five isotopes in 3D in a volume of 0.25 cm^3. Like similar non-isotope specific neutron techniques, the method does not require sample preparation and works with hazardous samples enclosed in containers.

Energy-resolved neutron imaging, utilizing neutron absorption resonances as unique 'finger-prints' of isotopes, allows to reliably determine the 2D areal-density distribution of isotopes with suitable resonances. Well-developed neutron cross-section analysis implemented in state-of-the-art neutron transmission data analysis codes [12, 13] allow to determine the areal densities of multiple isotopes

simultaneously, including considerations such as self-attenuation or resonance interference described by the Reich-Moore formalism [14]. At a short-pulse neutron source, such as the Los Alamos Neutron Science Center (LANSCE) [11], pixilated time-of-flight neutron detectors [10] enable therefore three-dimensional isotope density measurements as the number of nuclei of a given isotope can be measured per voxel using tomographic data-sets. Previous research has estimated the isotope density in two dimensional radiographs [15, 16], and eluded to the potential of this technique [17, 18]. However, the massive amount of neutron transmission analyses for each pixel recorded in a tomography dataset consisting of several tens or hundreds of rotations, strategies for proper background treatment to obtain reliable results and other obstacles have prevented full development of this intriguing technique. With this work, we demonstrate that three-dimensional isotope density measurements are possible with energy-resolved neutron imaging.

2. Energy-resolved Neutron Imaging Of Nuclear Fuel Slugs

Using energy-resolved neutron imaging, a U-20Pu-10Zr-3Np-2Am (weight percent) sample, an alloy researched for transmutation nuclear fuels [19], was characterized to obtain the bulk composition for comparison with mass-spectrometry. The sample consisted of a 20 mm long, 4.2 mm diameter U-20Pu-10Zr-3Np-2Am (weight percent) cast fuel slug contained in a double-walled steel container. The sample was prepared at Idaho National Laboratory where also mass spectrometry was performed (Table 1). The sample was mounted on a rotation stage and energy-resolved neutron imaging data was collected for 120 minutes per rotation for 65 rotations.

Considering only an active-area on the detector from pixels where the neutron beam traversed the sample volume (Figure 1, A), 50,000 (125 · 400) pixels required neutron transmission data analysis per sample rotation, resulting in 3.25 million total transmission-spectra fits. The SAMMY code [12] was used with cross section data for the isotopes ^{237}Np, ^{238}U, ^{239}Pu, ^{240}Pu, and ^{241}Am obtained from the ENDF/B-VIII.0 data base [20]. For conventional transmission measurements, the sample is generally several tens of meters away from the detector, such that sample induced background can be neglected [21]. In contrast, for imaging measurements, the sample position is as close as possible to the detector to reduce blurring resulting from the divergent beam. However, this sample position impacts the background in imaging applications and therefore the sample induced background needed to be properly accounted for to obtain reliable areal and volumetric densities. To accomplish this, a Ta foil was mounted on the detector window with a thickness of 100 µm, leading to opaque resonances. This allowed for reliable determination of the background, including sample contributions, by the transmission values at the bottom of these resonance dips in the transmission data.

Figure 1 shows an example of the data analysis for single pixels with fitted transmission for a pixel within the slug in B) and outside the slug in C). The total computing time for the data analysis of the tomographic data-set processing 3.25 million spectra on a desktop PC using 64 · 2.4 GHz CPUs was 16 days. The bulk composition was determined from the average density of the reconstructed sample volume. Table 1 shows the comparison of the results with the results of the mass spectrometry. The

maximum discrepancy for the four isotopes except ^{238}U is 0.08 g/cm^3, establishing the reliability of this method. The reason for the discrepancy of 1.8 g/cm^3 for ^{238}U lays in the properties of the ^{238}U resonance in the dataset. The analyzed energy range of 0.2 to 9 eV only provided a single ^{238}U absorption resonance at 6.67 eV. At a fractional density of ~9 g/cm^3 and cross sections >>10^3 barn, this led to insufficient non-zero transmission at resonance energies for a reliable data fit. Furthermore, the absorption resonance at 6.67 eV for ^{238}U has a comparatively narrow profile with respect to the other isotopes present and the resonance overlaps significantly in the non-zero transmission range with other resonances. Increasing the energy range for the analysis could mitigate this problem but was not feasible with the available resources for all 3.25 million datasets.

Table 1

Isotope densities from energy-resolved neutron imaging compared with those from mass spectrometry. For the neutron analysis, the factional density was computed by the average of the reconstructed sample volume, averaged over all voxels fully inside the sample with errors computed using the standard deviation of the voxel densities.

Isotope	Weight fraction from mass spectrometry [µg/g]	Fractional density from mass spectrometry [g/cm^3]	Fractional density from neutron analysis [g/cm^3]
^{234}U	<30	0.00	
^{235}U	1490	0.02	
^{236}U	113	0.00	
^{237}Np	24400	0.34	0.310(3)
^{238}U	639000	9.01	10.8(2)
^{239}Pu	166000	2.34	2.26(2)
^{240}Pu	26400	0.37	0.369(3)
^{241}Am	23000	0.32	0.314(3)
Zr	100000	1.41	
Total	980433	13.82	14.09

The large absorption cross section for thermal neutrons of ^{239}Pu made it impossible to utilize thermal neutrons for neutron tomography. Using the sample composition, the computed transmission at a thickness of 4.2 mm for 25 meV neutrons equates to 3.5%. For such opaque samples, the reconstruction leads to artefacts of the average voxel density, so-called ‘beam hardening’ [22]. However, at epithermal neutron energies (E > 0.4 eV) the cross-section drops such that significant fractions of the beam are transmitted and a reliable tomographic reconstruction is possible. Figure 2 shows a 3D rendering of the fuel slug resulting from neutron tomography by selecting time-of-flight neutrons only at the upper end of the thermal spectrum, with energies ranging from 0.1 to 0.2 eV. Several globular features are apparent.

The tomographic reconstruction of the densities of the aforementioned isotopes allowed further investigation of these features and greatly reduced densities for all isotopes were found at the locations of the globular features. This would indicate that the features are either casting voids or Zr-rich metallic inclusions (Zr did not provide neutron absorption resonances in the 0.2 to 9 eV energy range used for the measurements). With the slices of the tomographic reconstruction providing data similar to elemental maps provided by X-ray microprobe, but within the bulk of a sample, non-destructively, and for samples that have to be in containers such as nuclear fuels, this characterization guides destructive post irradiation examination by identifying where this sample should be cut for further investigations.

3. Summary

In summary, three-dimensional quantitative isotope density measurements on cm^3 sized volumes with sub-mm spatial resolution was demonstrated with the results in agreement to prior measurements using mass spectrometry. This technique extends the range of available elemental or isotope-density measurement techniques to the mm length scale. Applications may include characterization of fresh and irradiated nuclear fuels (as demonstrated here), dopant concentrations of large crystals for scintillator [16] or laser [23] applications, containing elements with suitable resonances for this technique. A combination of a short-pulsed neutron source with a pixilated time-of-flight neutron imaging detector and massive data analysis runs with state-of-the-art nuclear physics analysis code enabled this unique capability. While limited at the present time to large-scale pulsed neutron user facilities, the potential of laser-driven short pulse intense neutron sources [24] may provide this technique at other facilities within a decade.

4. Methods

At the pulsed spallation neutron source at LANSCE, 270 ns long (base-to-base) pulses of 800 MeV protons from a linear accelerator and proton storage ring produce neutron bursts at 20 Hz which are subsequently moderated. Collimation consisted of steel and borated polyethylene rings increasing from 2 cm inner diameter to 5 cm over a total length of 150 cm with a distance of ~750 cm from the smallest diameter of the collimator to the sample (see [25] for more details on the beam line). The neutrons in each pulse arrive at the detector sorted by their energy, with higher energy neutrons arriving first. The time-of-flight from the moderator to the detector allows with the calibrated distance between moderator and detector to compute the velocity and kinetic energy of the neutron [26]. Tabulated neutron interaction cross sections are available in databases such as ENDF [27]. Many isotopes, especially isotopes heavier than ~Zr, exhibit sharp increases in their neutron absorption cross section for specific neutron energies, so-called neutron absorption resonances [28–30]. Similar to optical spectroscopy, where an element can be identified by its optical emission or absorption spectrum, neutron resonance spectroscopy allows to identify isotopes present in transmission spectra by means of neutron resonance transmission analysis [31]. The neutron transmission T for neutrons of energy E is given by

$$T(E) = \frac{I_s(E) - I_{bs}(E)}{I_o(E) - I_{bo}(E)} = exp^{-\sum_i n_i \sigma_i(E)} \quad , \qquad (1)$$

whereby $I_s(E)$ is the intensity transmitted through the sample, $I_{bs}(E)$ the background with sample in beam, $I_o(E)$ the incident or open beam intensity and $I_{bo}(E)$ the background for the open beam. All of these intensities vary for each pixel of a 2D detector and therefore need to be measured pixel by pixel. In the exponent, the sum is running over each isotope present in the sample, with n_i the areal density of the i_{th} isotope, and $\sigma_i(E)$ the cross section of the i_{th} isotope for neutrons of energy E [21, 32]. For the purpose of isotope density measurements, the cross section is assumed to be known, leaving the areal density as the only variable during the analysis. This analysis has to be performed for each pixel of the detector where the sample is visible. In our case, a detector consisting of a multi-channel plate and a MediPix readout chip was utilized [10] to record ~3000 frames per 50 ms pulse of the neutron source with a pixel size of 55 µm. The field of view is 512 · 512 pixels or 28.16 · 28.16 mm^2.

Declarations

Acknowledgements

We gratefully acknowledge funding from the DOE/NE Fuel Cycle R&D program and provision of the sample material described here by Dr. R. Fielding, Idaho National Laboratory. We are indebted to Drs. K.J. McClellan (LANL) and M.A.M. Bourke for encouragement and valuable discussion as well as Dr. A.S. Tremsin (UC Berkeley) for technical support with the detector during the period of this project.

Author contributions

A.S.L. and S.C.V. conceived and conducted the experiments, performed the data-analysis and wrote the manuscript.

References

1. Beckhoff, B., Kanngießer, B., Langhoff, N., Wedell, R. & Wolff, H. *Handbook of practical X-ray fluorescence analysis*. (Springer Science & Business Media, 2007).
2. Durrant, S. F. Laser ablation inductively coupled plasma mass spectrometry: achievements, problems, prospects. *J. Anal. At. Spectrom.* **14**, 1385–1403 (1999).
3. Kelly, T. F. & Miller, M. K. Atom probe tomography. *Rev. Sci. Instrum.* **78**, 31101 (2007).
4. De Samber, B. *et al.* Three-dimensional elemental imaging by means of synchrotron radiation micro-XRF: Developments and applications in environmental chemistry. *Anal. Bioanal. Chem.* **390**, 267–271 (2008).

5. Kanngießer, B., Malzer, W. & Reiche, I. A new 3D micro X-ray fluorescence analysis set-up - First archaeometric applications. *Nucl. Instruments Methods Phys. Res. Sect. B Beam Interact. with Mater. Atoms* **211**, 259–264 (2003).
6. Miller, M. K. *Atom probe tomography: analysis at the atomic level*. (Springer Science & Business Media, 2012).
7. Baruchel, J., Buffiere, J.-Y. & Maire, E. X-ray tomography in material science. (2000).
8. Cnudde, V. & Boone, M. N. High-resolution X-ray computed tomography in geosciences: A review of the current technology and applications. *Earth-Science Rev.* **123**, 1–17 (2013).
9. Strobl, M. *et al.* Advances in neutron radiography and tomography. *J. Phys. D. Appl. Phys.* **42**, (2009).
10. Tremsin, A. S., Feller, W. B. & Downing, R. G. Efficiency optimization of microchannel plate (MCP) neutron imaging detectors. I. Square channels with10B doping. *Nucl. Instruments Methods Phys. Res. Sect. A Accel. Spectrometers, Detect. Assoc. Equip.* **539**, 278–311 (2005).
11. Lisowski, P. W., Bowman, C. D., Russell, G. J. & Wender, S. A. The Los Alamos National Laboratory Spallation Neutron Sources. *Nucl. Sci. Eng.* **106**, 208–218 (1990).
12. Larson, N. M. *Updated Users' Guide for SAMMY Multilevel R-matrix Fits to Neutron Data Using Bayes' Equation*. (1998).
13. Moxon, M. C., Ware, T. C. & Dean, C. J. REFIT-2009 A Least-Square Fitting Program for Resonance Analysis of Neutron Transmission. *Capture, Fission Scatt. Data Users' Guid. REFIT-2009-10 (UKNSFP243, 2010)* (2010).
14. Reich, C. W. & Moore, M. S. Multilevel formula for the fission process. *Phys. Rev.* **111**, 929–933 (1958).
15. Festa, G. *et al.* Neutron resonance transmission imaging for 3D elemental mapping at the ISIS spallation neutron source. *J. Anal. At. Spectrom.* **30**, 745–750 (2015).
16. Tremsin, A. S. *et al.* Real-time crystal growth visualization and quantification by energy-resolved neutron imaging. *Sci. Rep.* **7**, 1–10 (2017).
17. Kai, T. *et al.* Visibility estimation for neutron resonance absorption radiography using a pulsed neutron source. *Phys. Procedia* **43**, 111–120 (2013).
18. Hasemi, H. *et al.* Evaluation of nuclide density by neutron resonance transmission at the NOBORU instrument in J-PARC/MLF. *Nucl. Instruments Methods Phys. Res. Sect. A Accel. Spectrometers, Detect. Assoc. Equip.* **773**, 137–149 (2015).
19. Janney, D. E. & Papesch, C. A. *FCRD Transmutation Fuels Handbook 2015*. (2015).
20. Brown, D. A. *et al.* ENDF/B-VIII. 0: the 8th major release of the nuclear reaction data library with CIELO-project cross sections, new standards and thermal scattering data. *Nucl. Data Sheets* **148**, 1–142 (2018).
21. Schillebeeckx, P. *et al.* Determination of resonance parameters and their covariances from neutron induced reaction cross section data. *Nucl. Data Sheets* **113**, 3054–3100 (2012).

22. Zawisky, M., Bastürk, M., Rehacek, J. & Hradil, Z. Neutron tomographic investigations of boron-alloyed steels. *J. Nucl. Mater.* **327**, 188–193 (2004).
23. Kmetec, J. D., Grund, C. J., Kubo, T. S. & Kane, T. J. Laser performance of diode-pumped thulium-doped Y_3Al_5O_12, (Y, Lu)_3Al_5O_12, and Lu_3Al_5O_12 crystals. *Opt. Lett.* (1994) doi:10.1364/ol.19.000186.
24. Fernández, J. C. *et al.* Laser-plasmas in the relativistic-transparency regime: Science and applications. *Phys. Plasmas* **24**, 56702 (2017).
25. Mocko, M., Muhrer, G. & Tovesson, F. Advantages and limitations of nuclear physics experiments at an ISIS-class spallation neutron source. *Nucl. Instruments Methods Phys. Res. Sect. A Accel. Spectrometers, Detect. Assoc. Equip.* **589**, 455–464 (2008).
26. Windsor, C. G. *Pulsed Neutron Scattering*. (Taylor & Francis, London, 1981).
27. Chadwick, M. B. ENDF nuclear data in the physical, biological, and medical sciences. *Int. J. Radiat. Biol.* **88**, 10–14 (2012).
28. Bohr, N. Neutron capture and nuclear constitution. (1936).
29. Breit, G. & Wigner, E. Capture of slow neutrons. *Phys. Rev.* **49**, 519 (1936).
30. Lamb, W. E. Capture of neutrons by atoms in a crystal. *Phys. Rev.* (1939) doi:10.1103/PhysRev.55.190.
31. Postma, H. & Schillebeeckx, P. Neutron resonance capture and transmission analysis. *Encycl. Anal. Chem. Appl. Theory Instrum.* (2006).
32. Harvey, J. *Experimental neutron resonance spectroscopy*. (Elsevier, 2012).

Figures

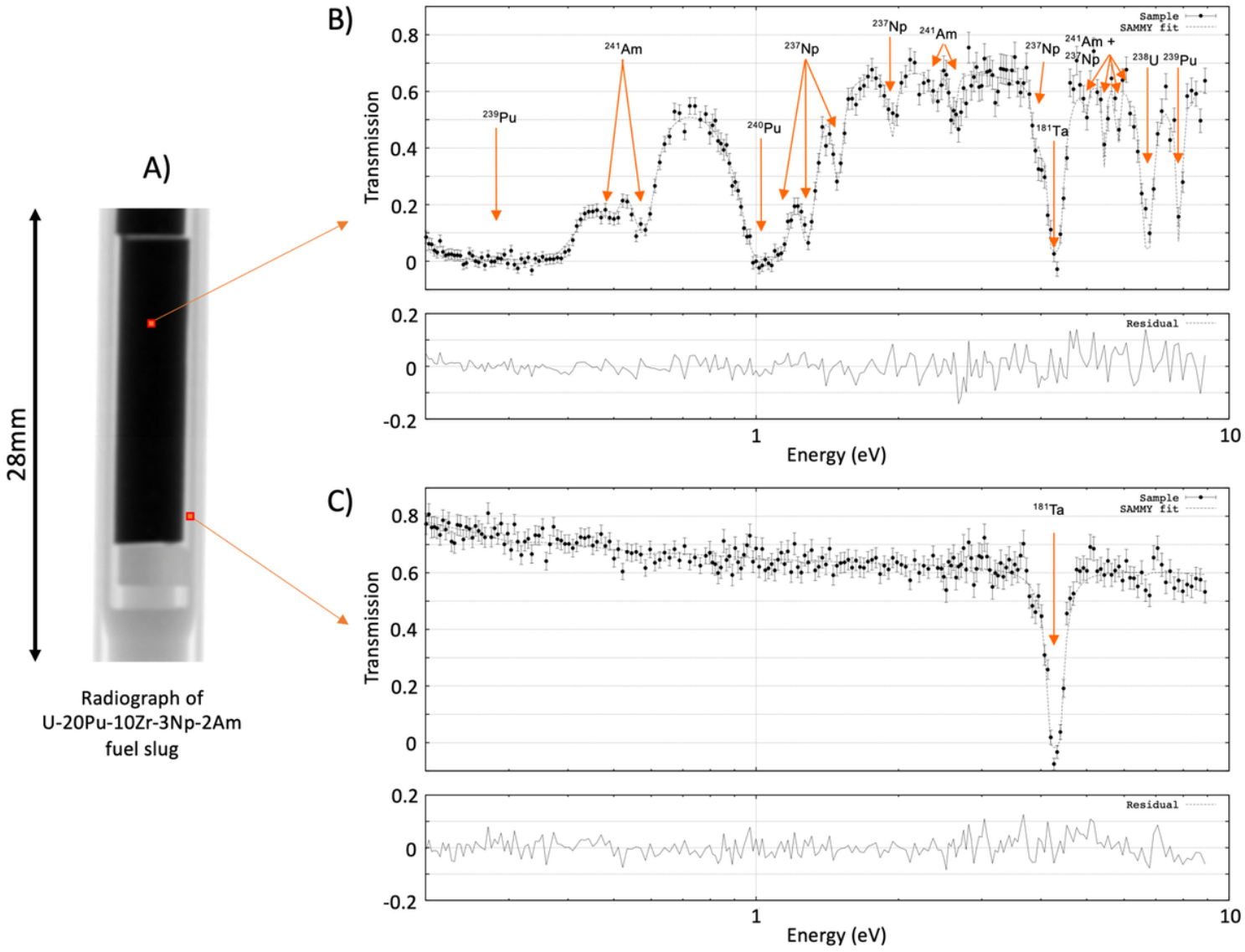

Figure 1

Thermal neutron radiograph A) with single pixel data for isotope concentration measurement with a fit of the transmission data inside (B) and outside (C) the sample. Arrows mark the resonances of several isotopes and the difference curves between experimental data and fit are shown.

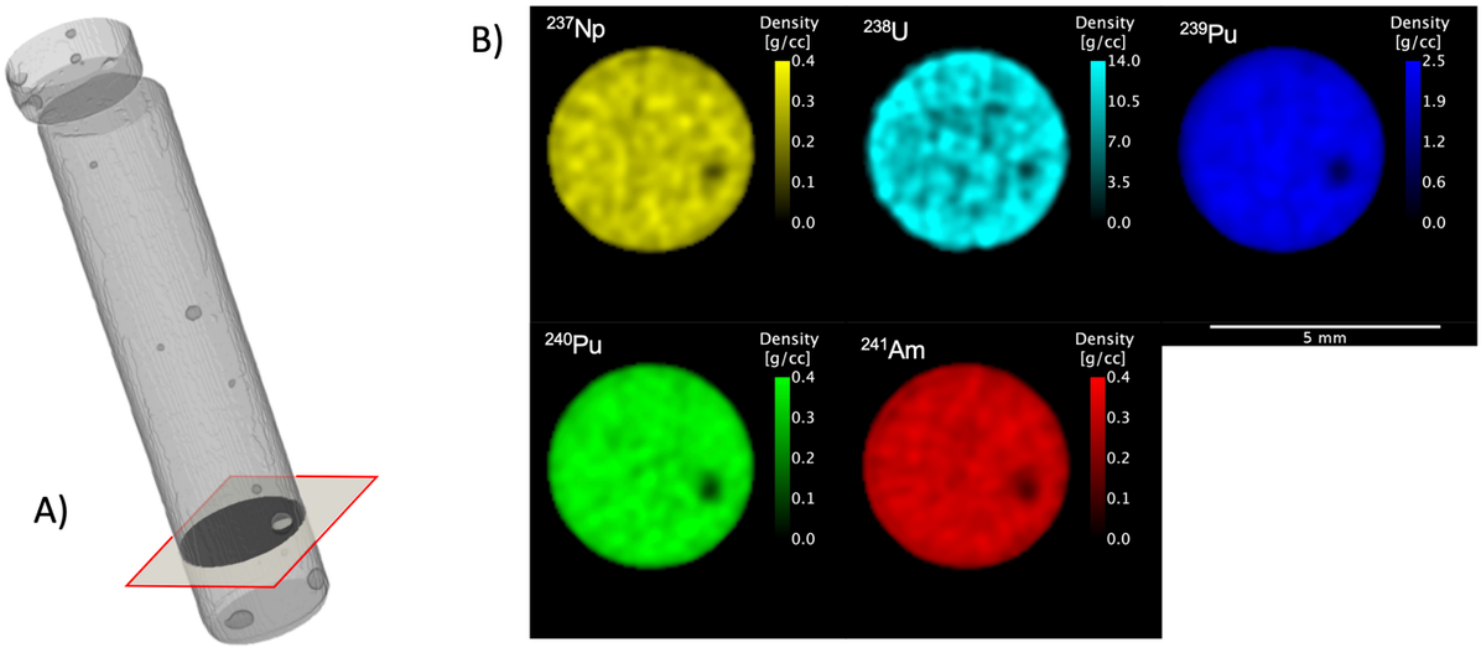

Figure 2

Volumetric reconstruction using epithermal neutrons of the U-20Pu-10Zr-3Np-2Am sample in A) with indicated region in red for CT slice of the volumetric densities of individual isotopes as shown in B).